Heat-induced effective exchange in magnetic multilayers

Michael Hunziker and Martin Landolt
Laboratorium für Festkörperphysik der ETH Zürich, CH-8093 Zürich, Switzerland
(Received 17 August 2000; revised manuscript received 2 March 2001; published 13 September 2001)

Two ferromagnetic Fe layers separated by an amorphous semiconducting spacer layer are antiferromagnetically exchange coupled. The sign and strength of the exchange coupling between thin Fe films across amorphous ZnSe of variable thickness is determined using spin-polarized secondary electron emission and Kerr effect. The coupling strength is found to strongly increase upon heating at low temperatures. Electrical transport measurements on bilayers of amorphous ZnSe and Fe give evidence for donor states at or near the interfaces between the metal layers and the semiconducting spacer layer. Based on these states we present an interesting description of interlayer exchange coupling: the molecular-orbital model. The donor states are assumed to be weakly bound. They overlap across the spacer layer and form large molecular orbitals. The energies of these orbitals depend on the spin configuration of the electrons and therefore determine the exchange coupling. Thermal repopulation of the levels yields a positive temperature coefficient of the coupling. The results of an approximate calculation are found to well reproduce the experimental observations.

DOI: 10.1103/PhysRevB.64.134421 PACS number(s): 75.30.Et, 75.70.Cn

I. INTRODUCTION

The interaction between two magnetizations or, in other words, a *magnetic coupling*, is a manifold phenomenon to study: A magnetic coupling is not only given by its size, there is also an angle to be determined, as magnetizations may be described as vectors. The phenomenological, effective coupling strength J thus may be defined by the exchange energy of the interaction E_{ex} as

$$E_{ex} = -J\frac{\mathbf{M_1}\cdot\mathbf{M_2}}{|\mathbf{M_1}||\mathbf{M_2}|}, \tag{1}$$

where $\mathbf{M_1}$ and $\mathbf{M_2}$ denote the two interacting magnetizations. A positive and negative sign of J causes the magnetizations to stand parallel and antiparallel, respectively.

A magnetic coupling may either be mediated by a magnetostatic field or across electron wave functions situated between the magnetizations. Of course, the mediation across electron states is the more interesting interaction. It can be of fairly long range and it allows us to study the behavior of electrons in solids.

The sign of the interaction across a free-electron gas in general oscillates with increasing distance between the magnetic objects.[1] In the case of more than two objects involved in a magnetic interaction, for example in a two- or three-dimensional lattice of spins, the contributions to the interaction annihilate because of frustration. Therefore a multilayer consisting of two-dimensional ferromagnetic layers separated by nonferromagnetic spacer layers is an ideal system to study magnetic coupling effects. In multilayers the ferromagnetic layers are separated by a well defined distance and one component of the interaction remains.

In multilayers with *metallic* spacer layers such as Cr or Cu the magnetizations of the ferromagnetic layers were discovered to be coupled.[2] The sign of the interaction was found to oscillate with rising spacer thickness[3,4] while its size was observed to decrease quite slowly. The interaction across the spacer layer is mediated by the gas of free electrons, either by a spin-dependent confinement of the free electrons between the ferromagnetic layers[5] or by a Ruderman-Kittel-Kasuya-Yosida (RKKY)-type interaction.[6,7] Finally the two explanations turned out to be equivalent.

Multilayers with amorphous, *semiconducting* spacer layers evaporated at low temperatures were also found to be exchange coupled.[8] Mainly, at spacer thicknesses in the range of about 20 Å antiferromagnetic coupling is observed—with the most remarkable property that the coupling strength increases reversibly with rising temperature.[9] Therefore this coupling was labeled ''heat-induced exchange.'' It could be observed so far for the spacer materials Si,[8,9] Ge,[10] and, as presented in this paper, for ZnSe.[11]

As heat-induced exchange coupling can be observed even at low temperatures where no free electrons are present in the semiconductor it becomes clear that a new theoretical concept is needed in order to understand the coupling mechanism. Briner in his considerations very early relied on defects in the semiconductor material,[12] Walser later suspected the relation of defects with the interfaces.[13] In this report we present transport measurements along Fe/ZnSe interfaces which give strong evidence that the exchange coupling is mediated by localized electron states near or at the interfaces between semiconductor and ferromagnet.[14] The existence of these states is the key to the understanding of the coupling mechanism. Therefore we introduce a model which relies on shallow donor states near the interfaces which interfere across the spacer layer and thus transmit the exchange coupling.[15] The concept of this coupling mechanism is unconventional in magnetism. However, the interaction between the electron spins is quite analogue to the spin interaction in hydrogen molecules. Therefore we call it the ''molecular-orbital model.'' The results of a roughly approximated calculation are found to very well agree with the experimental data and to be robust upon variation of the few free parameters.

II. HEAT-INDUCED EXCHANGE COUPLING IN Fe/ZnSe MULTILAYERS

A. Why Fe/ZnSe multilayers?

Heat-induced exchange coupling has been found for the amorphous spacer materials Si and Ge. An important prerequisite is that the multilayers are prepared at temperatures around 30 K. In this section, we present measurements on amorphous Fe/ZnSe/Fe trilayers which yield heat-induced exchange coupling as well. ZnSe is a compound material with ionic binding and with a much larger energy gap than the one of covalent Si and Ge. It becomes clear that this coupling effect does not depend on a specific spacer material, it rather is a general magnetic behavior of ferromagnet-semiconductor multilayers. While Si and Ge react very easily with Fe, which has been used for the ferromagnetic layers in all previous and present measurements, Fe and ZnSe very weakly intermix even at room temperature.[16] Nevertheless, preparation at low temperatures also is a prerequisite for the occurrence of the exchange coupling in Fe/ZnSe multilayers. We thus have got an indication that low temperature is quite decisive and not only inhibits the chemical reaction at the interfaces.

B. Experiment

The measurements are performed on trilayers of amorphous Fe/ZnSe/Fe which are evaporated onto a crystalline Cu substrate. The amorphicity of the layers is checked by low-energy electron diffraction (LEED). As we apply surface sensitive methods the magnetization of the bottom ferromagnetic layer needs to be well known during the measurement. It needs to be a ''magnetic driver,'' a layer with a hard magnetization of which the direction is well defined. Therefore a thick and crystalline Co layer is placed between the substrate and the bottom Fe layer in order to make the magnetization of the bottom layer hard and to give it a well defined anisotropy. In detail, we first evaporate 70 Å Co onto the Cu substrate. An elevated temperature of about 90 °C during the evaporation improves the crystalline anisotropy and enlarges the coercivity of the magnetization. 6 Å Fe completes the bottom ferromagnetic driver. The ZnSe spacer layer with variable thickness is evaporated at room temperature while we cool to 30 K for the completion to the sample with 15 Å Fe. We note that it is crucial to produce the top Fe layer at temperatures below 150 K in order to make the coupling occur. Further, low temperatures during the ZnSe evaporation and a brief annealing at 150 K after completion of the multilayer favor the coupling effect.

ZnSe is evaporated from powder (Alfa, 99.999%) in W crucibles whereas Fe (Alfa, 99.9985%) and Co (Alfa, 99.9975%) are evaporated from rods. The evaporation rate is kept at about 2 Å/min. ZnSe evaporated onto a sapphire surface below 70 °C is reported to grow amorphously; crystallization is to be expected at 170–210 °C.[17] The sample preparation as well as the measurements are performed in an ultrahigh vacuum (UHV) chamber with base pressure below 1×10^{-10} mbar. The cleanliness of the sample is checked by standard Auger electron spectroscopy (AES). Within the resolving power of AES we do not find any interdiffusion to occur.

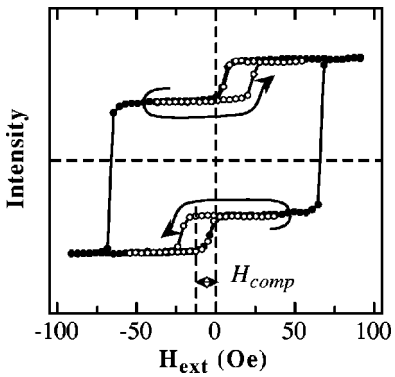

FIG. 1. MOKE signal of the multilayer 15 Å Fe/25 Å ZnSe/6 Å Fe/70 Å Co/Cu(100) (full dots). The open dots indicate minor loops originating from the top layer only.

We use spin polarized secondary electron emission (SPSEE) to probe the angle of the coupling depending on the spacer thickness. A 1–5-keV unpolarized electron beam produces a cascade of secondary electrons on the sample surface. The two in-plane components of the spin polarization **P** are measured in a Mott detector. **P** is proportional to the magnetization of the surface,[18,19] with the two components defined as $P_i=(N_i\uparrow-N_i\downarrow)/(N_i\uparrow+N_i\downarrow)$, where $N_i\uparrow$ and $N_i\downarrow$ are the number of electrons with spin parallel and antiparallel to the chosen quantization axis $i=x,y$, respectively. Hence we monitor the magnetization of the top Fe layer and, as the bottom ferromagnetic layer is hard with a well defined anisotropy, we can determine the angle between the magnetizations. With the knowledge of the magnetizations direction we then apply magneto-optical Kerr effect (MOKE) to determine the coupling strength J. A laser beam of linearly polarized light is reflected on the sample. The polarization of the reflected beam rotates due to the magnetization of the sample. MOKE is less surface sensitive than SPSEE which allows us to study the magnetizations of the top and the bottom ferromagnetic layers at the same time. The $M(H)$ response depicted in Fig. 1 represents a typical MOKE measurement on a Fe/ZnSe/Fe/Co multilayer. The horizontal shift between the major hysteresis loop originating from the bottom layer and the minor loops originating from the top layer is identified as the compensation field H_{comp}. H_{comp} compensates the coupling strength J, as defined in Eq. (1), and therefore is directly proportional to J,

$$J=t_{Fe}M_S H_{comp}. \tag{2}$$

t_{Fe} and M_S are the thickness of the top Fe layer and its saturation magnetization, respectively. This equation can easily be derived: at H_{comp} the magnetostatic energy of the top Fe layer $E_{stat}=V_{Fe}M_S H_{comp}$ compensates the coupling energy $E_{coupl}=JA_{Fe}$, where V_{Fe} and A_{Fe} denote the volume and the area of the top Fe layer, respectively.

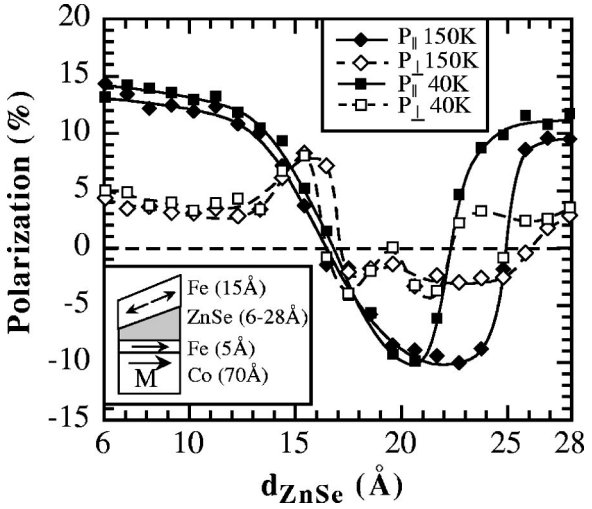

FIG. 2. Spin polarization P of secondary electrons at remanence of the top Fe layer of an Fe/a-ZnSe(wedge)/Fe sample deposited on a 70-Å Co/Cu(100) substrate, versus ZnSe spacer thickness. In-plane components parallel and perpendicular to the magnetizing field are shown. The change between the behavior at 40 and 150 K is fully reversible.

C. Results

First we study the spacer-thickness dependence of the exchange coupling. To do so we evaporate a wedge-shaped ZnSe layer with a thickness between 6 and 28 Å. The surface magnetization is monitored along the wedge measuring the spin polarization at remanence by SPSEE. As shown in Fig. 2, we find a thickness range around 20 Å where the sign of the polarization is negative, above and below a positive sign prevails. The sign of the polarization not necessarily corresponds with the sign of the coupling. While negative polarization (antiparallel alignment of the magnetizations) always stands for antiferromagnetic coupling, positive polarization (parallel alignment) is ambiguous; it may stand for ferromagnetic or zero coupling. MOKE measurements yield strong ferromagnetic coupling at small spacer thicknesses while weak or zero coupling is found at large spacer thicknesses. Already the data of Fig. 2 give evidence for a spectacular temperature behavior: The thickness range where antiferromagnetic coupling occurs *reversibly* broadens with rising temperature, mainly towards larger spacer thicknesses. Or, focusing on a fixed spacer thickness around 24 Å, the antiferromagnetic coupling may be switched on and off by temperature.

Measuring the coupling strength in the ''switching'' thickness range we observe heat-induced temperature behavior more accurately. We measure H_{comp} and derive J from Eq. (2). As shown in Fig. 3, MOKE measurements reveal the coupling strength to increase upon heating until it saturates. We emphasize that this behavior is strictly reversible. Considering the temperature behavior for different spacer thicknesses with ascending order one observes a decrease of the coupling strength at thermal saturation. At a spacer thickness of 30 Å a reversible switching from ferromagnetic coupling at 20 K to antiferromagnetic coupling above 50 K can be found. The magnitude of J is found to be small, it lies in the range of 10^{-6} Jm^{-2}.

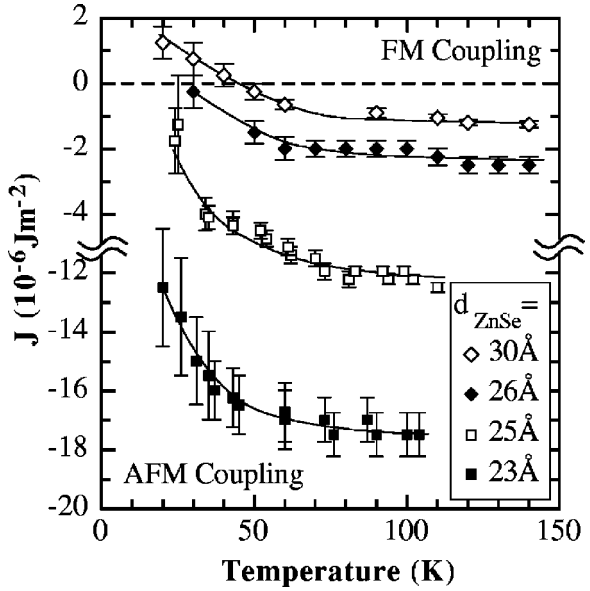

FIG. 3. Coupling strength J versus temperature for a variety of spacer thicknesses. We measure H_{comp} by MOKE and derive J with Eq. (2). In the temperature range chosen, all temperature dependences are fully reversible. We note that the coupling of samples with larger spacer thicknesses undergoes a sign change. The error bars originate from the quality of the minor loops.

A careful look at the data of the polarization measurements and the data of the coupling strength measured by MOKE reveals that they are not perfectly consistent. We ascribe this to the fact that the MOKE measurements have been recorded later in the course of the experiments. The thickness range where antiferromagnetic coupling occurs is found to slightly shift with the time of operation of the ZnSe evaporators.

Important information for the discussion of the coupling mechanism is the temperature at which the coupling irreversibly disappears. The reversibility of the temperature behavior is restricted to temperatures below 200 K. Above, an irreversible transition takes place; see Fig. 4. The negative sign of the coupling disappears and ferromagnetic coupling prevails which then hardly depends on temperature.

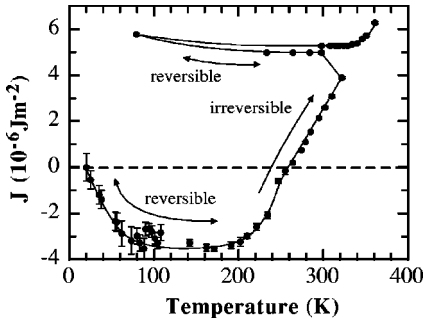

FIG. 4. Coupling strength J versus temperature measured on a multilayer Fe/ZnSe/Fe/Co with spacer thickness $t_{ZnSe}=30$ Å. Upon heating to above 200 K we observe an irreversible transition to ferromagnetic coupling with a weak temperature dependence.

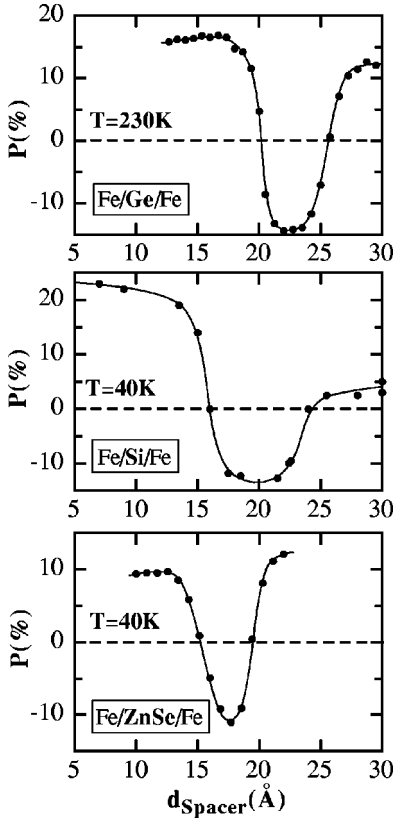

FIG. 5. Compilation of the spacer-thickness dependence of the surface polarization in multilayers with Ge, Si, and ZnSe spacers (from Refs. 10, 8, and 11). The thickness range of antiferromagnetic coupling follows more the dielectric constant of the semiconductor ($\varepsilon_{Ge}=16$, $\varepsilon_{Si}=11.2$, $\varepsilon_{ZnSe}=9.2$) than the semiconductor's energy gap ($\Delta E_{Ge}=0.67$ eV, $\Delta E_{Si}=1.1$ eV, $\Delta E_{ZnSe}=2.6$ eV) (Ref. 20).

D. Discussion

The multilayer Fe/ZnSe/Fe/Co is a very suitable system to characterize heat-induced exchange coupling. The combination of a remanent and soft magnetization of the top Fe layer with a hard magnetization of the magnetic driver allows a direct and accurate measurement of the coupling strength *J*. Remarkably, the sample exhibits exchange coupling despite its almost insulating spacer. Moreover, the coupling occurs even at 40 K. The characteristic temperature behavior with an increasing size of *J* below 100 K and a saturation above is a suitable touchstone for the results of theoretical models.

The irreversible transition at about 250 K is another feature which helps to unveil the coupling mechanism. We know that Fe and ZnSe are chemically inert which is supported by the fact that the remanent magnetization of the top Fe layer survives the transition. Therefore, the occurrence of the transition gives strong evidence that small structural changes may destroy the coupling phenomenon. The fact that the transition takes place at 250 K while the whole multilayer except the top Fe layer has been evaporated at room temperature gives an indication that these structural changes occur at the interfaces between ZnSe and Fe. One might think of *defect states at the interfaces* to be involved with the coupling mechanism.

In order to discuss the coupling phenomenon more generally we compare the present data with the data measured on multilayers with Si[8,9] and Ge[10] spacers. First of all, the antiferromagnetic coupling occurs across all mentioned spacer materials in the same range of spacer thicknesses; compare Fig. 5. We note that the thickness range does not depend on the size of the semiconductors energy gap, rather a dependence on the dielectric constant ε may be observed.

Multilayers with Ge spacers exhibit the necessity of an annealing at 190 K in order to make the coupling occur. This observation already has given rise to the suspicion that the interfaces play an important role for the mediation of the coupling.[13] Furthermore, at that point of investigation it was questioned whether the ferromagnetic layers were separated by a pure semiconductor layer or rather a compound layer was formed, due to the reactivity between Fe/Si and Fe/Ge, respectively. Therefore, x-ray photoelectron spectroscopy (XPS) measurements have been performed on Fe/Si and Fe/Ge bilayers to examine the layer structures and the chemical interface properties.[21] During preparation of the sample and measurement the temperature was kept low such that the conditions were similar to the ones of the coupling experiments. Between the Fe layer and the Si (Ge) substrate a compound layer of homogeneous composition was detected while a Si (Ge) layer on top of a Fe substrate could not be observed to intermix. The thickness of the compound layer at the Fe/Si (Fe/Ge) interface at 30 K is small enough such that in the trilayers, where the coupling has been observed, the ferromagnets still are separated by a pure semiconductor. Obviously, the thickness of the pure spacer layer is reduced compared to its nominal value. Finally, the resolving power of XPS is too low to observe any change of the interface properties while annealing.

To reveal the coupling mechanism, however, some concepts can be excluded. All attempts to explain the mediation of heat-induced exchange coupling by free electrons (which in the context of this paper means quasifree or band electrons) should be abandoned because of the occurrence of the coupling at low temperatures and because of the lack of a dependence on the size of the semiconductor's energy gap. Moreover, free electrons would not be sensitive to small structural changes and therefore no irreversible transition would be observed. ''Metal-induced gap states,'' free electrons which leak from the Fe into the semiconductor, would not be annihilated by such structural changes either. So far, the mediation via defect states remains the favorite explanation. Evidence for such defect states will be unveiled in the following section, and it will be the basis for a model description of the coupling mechanism.

III. TRANSPORT MEASUREMENTS: EVIDENCE FOR INTERFACE DEFECT STATES

A. Transport in amorphous semiconductors

Some features of the heat-induced coupling give rise to the *assumption* of defect states to be the key to the understanding of the coupling mechanism. Assumption is not evidence. The location, the density, and the relative position on

the energy scale of the defect states are needed to be known in order to understand the interaction.

To answer these questions we present transport measurements which have been performed along bilayers consisting of one ferromagnetic metal layer and one amorphous semiconductor layer. In amorphous semiconductors with the Fermi energy E_F lying in the range of localized defect states, the conduction may be described by two different mechanisms.[22] First, the current may evolve across the defect states by variable range hopping and second, electrons may be excited into the conduction band and establish a current carried by free electrons. The energy gap between the conduction-band edge E_C and the center of the defect levels E_S ($\sim E_F$ in our case) even for shallow donors is in the range of 10 meV. Therefore at low temperatures the conductivity depends on $N(E_F)$, the density of the defect states at the Fermi level, while at higher temperatures the energy gap $E_C - E_F$ rules the current.

In heterostructures the influence of the neighboring metallic layers on the formation of interface defect states cannot be neglected. The specific conductivity of these metal layers is enormous compared to the one of semiconductors, especially at low temperatures. In order to observe the contribution of the semiconductor to the total current of a metal-semiconductor heterostructure we keep the thickness of the metal layer in the range of a few monolayers.

For a mathematical description of the mentioned conductivities we follow the considerations by Mott and Davis.[22] They describe variable range hopping in noncrystalline semiconductors. The conductivity for a hopping current in a *three-dimensional* semiconductor is given by

$$\sigma_{3D}(T) = \sigma_{0,3D}(T)\exp(B_{3D}T^{-1/4}), \tag{3}$$

where $\sigma_{0,3D} = 2e^2 N(E_F) R^2 \nu_{ph}$ and $B_{3D} = (24\alpha^3)/[\pi N(E_F)k]^{1/4}$. $R = (3/2)^{1/4}[\pi\alpha N(E_F)kT]^{-1/4}$ is the mean hopping distance, ν_{ph} the electron-phonon interaction constant, and α the decay constant of the localized states. For a *two-dimensional* current evolving in thin layers or along surfaces and interfaces Eq. (3) is slightly altered,

$$\sigma_{2D}(T) = \sigma_{0,2D}(T)\exp(B_{2D}T^{-1/3}) \tag{4}$$

with

$$\sigma_{0,2D} = 2e^2 N(E_F) R^2 \nu_{ph},$$

$$B_{2D} = (28\alpha^2)/[9\pi N(E_F)k]^{1/3},$$

and

$$R = (3/2)[\pi\alpha N(E_F)kT]^{-1/3}.$$

The conductivity caused by free electrons which are thermally excited from defect states follows the familiar excitation law

$$\sigma_{exc}(T) = C\exp\left(-\frac{E_C - E_F}{kT}\right), \tag{5}$$

where C is a parameter which depends on the details of the electronic structure and the mean free path. We assume, as a first approximation, that if a metal layer has percolated its conductivity is temperature independent.

B. Experiment

We perform our measurements on a sapphire substrate as depicted in Fig. 6. The sapphire surface is cleaned by sputtering with Ar. Onto this surface two Au electrodes are evaporated which are separated by a gap of 3 mm width and 30 μm length. The Au electrodes are contacted by thin Cu wires. The sapphire is fixed onto a Cu block for temperature control in the range of 20–450 K. The temperature is measured by a cromel-alumel thermocouple.

For the semiconductor layer we use ZnSe, for the metal layers Fe or Co are used. We note that Fe and ZnSe as well as Co and ZnSe are known to hardly intermix at the interfaces[16,23] and not to form any compound layers with particular electronic properties. To achieve thin layers with a similar consistency as used in the coupling experiments we work at UHV conditions and we grow the heterostructures the same way, by molecular-beam epitaxy onto the substrate surface held at 30 K. For details see Sec. II B.

As we are investigating metastable structures it is of decisive importance to clearly distinguish between reversible and irreversible thermal behavior. Therefore in order to properly analyze the temperature dependences we introduce an annealing temperature T_i. We heat the sample up to an arbitrarily chosen T_i and measure the temperature dependence of the conductivity with decreasing temperature, ''freezing'' the sample. In order to vary T_i we run heating and cooling cycles of conductivity measurements where the annealing temperature increases on each cycle. Since the bilayer samples are very inhomogeneous we consider the absolute conductivity instead of the specific one.

C. Results

In bilayers, a current may run along the bottom layer, the top layer, along the interface, or along a combination of all the three. Therefore, in order to determine the various contributions to the current, we first examine the different layers separately.

A pure ZnSe layer of 150 Å thickness evaporated at 30 K is found to be completely *insulating* at all temperatures up to 450 K, i.e., the conductivity is below $10^{-11}\ \Omega^{-1}$ which is our detection limit; compare Fig. 7, full dots.

A pure Fe layer of 4 Å thickness evaporated at 30 K on top of the sapphire substrate exhibits a measurable conductivity; see Fig. 7, empty dots. The conductivity behaves like an amorphous, two-dimensional semiconductor — the data can be fitted by Eq. (4) quite accurately. Assuming $\alpha^{-1} = 10$ Å, which is somewhat arbitrary, we find $N(E_F) = 2.5 \times 10^{12}\ \mathrm{eV}^{-1}\ \mathrm{cm}^{-2}$ to remain constant upon annealing.

In order to examine the interface properties between Fe and ZnSe we study bilayers of three configurations. First, a thin Fe layer on top of a ZnSe bottom layer (4 Å Fe/130 Å ZnSe), second, a thicker Fe layer on ZnSe (18 Å Fe/150 Å ZnSe), and third, an inverse bilayer consisting of a thin Fe layer covered by ZnSe (60 Å ZnSe/12 Å Fe). The results are given in Fig. 8, upper,

center, and bottom panels, respectively.

The measurements provide manifold results. First, we analyze what happens to a thin Fe layer on top of ZnSe, as shown in the top panel. We start at 30 K with zero conductivity. At all temperatures the conductivity behaves strictly like an amorphous, two-dimensional semiconductor. While at low temperatures the conductivity slightly decreases upon annealing, a sharp and large transition *reduces* the conductivity at 250 K. Above, a rather moderate annealing process continues.

In contrast, the thicker Fe layer (center panel) starts at 30 K with a finite conductivity. At low temperatures a semiconductorlike behavior is found after subtraction of a constant value of $\sigma_m = 5 \times 10^{-2}\ \Omega^{-1}$. However, no annealing process is visible. At 250 K an irreversible transition occurs as well, but this transition sharply *enhances* the conductivity. After the transition the temperature coefficient of the conductivity is negative and a moderate annealing process takes place.

The inverse bilayer with a thin Fe bottom layer (bottom panel) behaves quite similar to the bilayer with the thin Fe layer on top. The effect of the annealing at low temperatures is smaller, as well as the one of the transition at 250 K. After the transition no further annealing is observed until at around 450 K where crystallization processes of ZnSe start to play a role.

During the evaporation process of this particular layer a truly remarkable feature is observed: The coverage of the ground Fe layer by ZnSe enhances the conductivity by three orders of magnitude, even if ZnSe on its own has been measured to be insulating. We state that in all measurements the data do hardly depend on the thickness of the ZnSe layers.

The transition at 250 K, which occurs for all measured Fe-ZnSe bilayers, is the most remarkable result, of course. In order to get more information about the origin of this transition we alter the bilayer: First, we roughen the interface of a Fe/ZnSe bilayer and second, we study bilayers with Co replacing Fe.

In order to produce a bilayer with a rough interface, 155 Å ZnSe are sputtered with Ar for a few seconds at 2 kV. Then the sample is completed by 18 Å Fe. The data of the conductivity measured on this sample are given in Fig. 9 by empty dots. For comparison, the data measured on the same but unsputtered sample, already presented in Fig. 8, center panel, are given again by full dots. The results of this measurement reveal that the transition temperature strongly depends on the roughness of the interface. The transition of the rough sample is shifted to about 350 K. Furthermore, σ_m is reduced and the temperature dependence of the conductivity is less pronounced.

Finally we perform measurements on Co/ZnSe bilayers. Analog to the measurements on Fe/ZnSe we evaporate a 4-Å- and an 18-Å-thick Co layer on top of ZnSe holding the sample at 30 K in each case. The results, which are shown in Fig. 10, exhibit a slightly different behavior compared to the data measured on Fe/ZnSe. On one hand, already 4 Å Co (upper panel) provoke a nonzero conductivity at low temperature. On the other hand, the conductivity for 18 Å Co (lower panel) shows a negative temperature coefficient already for an as-grown sample. However, both samples undergo a transition at 250 K, with decreasing conductivity in the case of a thin Co layer and increasing conductivity for 18 Å Co.

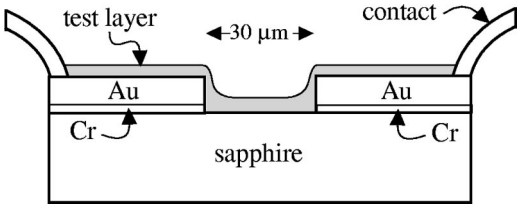

FIG. 6. Sample substrate as described in the text.

D. Conclusions

In a heterostructure consisting of two well separated layers the current may propagate along three channels: Along one of the two layers and along the interface. In the case of Fe-ZnSe bilayers the contribution of the ZnSe layer to this propagation is found to be zero, even at room temperature. This result agrees with the measurements on amorphous ZnSe performed by Lim and Brodie.[17] They found for samples, which were annealed at 140 °C, a density of defect states of about $N(E_F) \sim 10^{17}\ \mathrm{eV}^{-1}\ \mathrm{cm}^{-3}$. This translates in the case of a thin film of 130 Å thickness to $N(E_F) \sim 10^{11}\ \mathrm{eV}^{-1}\ \mathrm{cm}^{-2}$. The conclusion is straightforward: The energy gap of ZnSe is too large and its density of defect states is too low such as a measurable current could be established.

The conductivity of a thin Fe layer on top of the sapphire substrate behaves like an amorphous, two-dimensional semiconductor. The current thus must propagate along the Fe layer hopping from one site to another. We conclude that Fe on top of the sapphire surface grows in a distribution of grains. As the conductivity of a Fe/ZnSe bilayer reveals a similar behavior, Fe on top of ZnSe must grow similarly. Thin Fe layers exhibit zero conductivity towards 0 K which indicates that the grains are well separated from each other. Further, the slight reduction of the conductivity upon annealing may be attributed to a contraction of the Fe grains which also widens the gaps between them. Finally, thicker Fe layers or Co layers on a ZnSe bottom layer exhibit a semiconductorlike conductivity after subtraction of a ''metallic'' offset σ_m. In this case the growth still yields grains, however, they are connected to each other.

The large irreversible transition at 250 K measured on Fe-ZnSe bilayers deserves particular attention. This transition occurs neither in pure ZnSe layers nor in pure Fe layers; compare Fig. 7. Therefore we conclude that the origin of this transition is located at the *interface*. Possible coagulation effects, which could dramatically contract the Fe grains and thus reduce the conductivity, can be excluded. The reason is the occurrence of the transition in inverse bilayers where the Fe grains are covered by ZnSe and therefore have no degrees of freedom for a dramatic deformation. Furthermore, at 250 K no intermixing between Fe and ZnSe is expected to occur.

The origin of the transition is unveiled by the behavior of the conductivity: In the case of samples with thin Fe layers the transition leads to a reduction of the conductivity

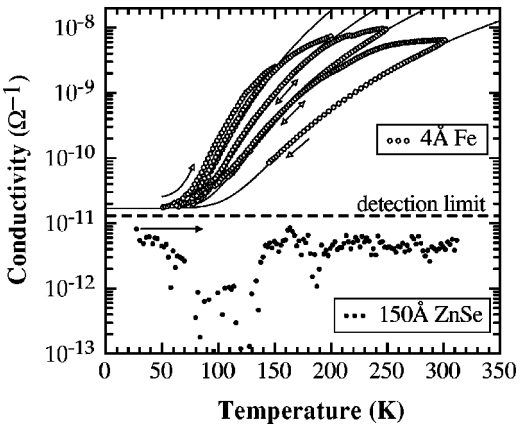

FIG. 7. Conductivity vs temperature of 150 Å ZnSe (full dots) and 4 Å Fe (empty dots). In two separate experiments the layers are evaporated at 30 K onto a sapphire substrate. The measurement on the Fe layer are performed by stepwise annealing, the course of the experiment is indicated by arrows. The full lines are best fits according to Eq. (4).

whereas on samples with thicker Fe layers the conductivity is sharply enhanced. We conclude that at temperatures below the transition *localized electron states* are present at the interface between Fe and ZnSe which disappear upon annealing at 250 K. In the case of thin Fe layers where the Fe grains are disconnected and the conductivity is in the hopping regime these states provide additional hopping sites. The conductivity is reduced when they disappear. In the case of thicker Fe layers where the Fe grains are connected and band electrons dominate the conductivity these localized states may act as traps and scatter the free electrons. Thus a reduction of these traps enhances the total conductivity.

These conclusions are supported by a quantitative analysis of the data. We fit the data with Eq. (4), where we set $\alpha^{-1}=10$ Å, which has been found to be appropriate for defects in amorphous Si,[22] and which in our case is assumed to not alter upon annealing. The results are given in Table I. For the thin Fe layers (top and bottom sections) best fits before and after the transition are available. The density of defect states which is lost by the transition is about $\Delta N(E_F)\approx 1\times 10^{13}$ eV^{-1} cm^{-2}. We neglect the complexity of a granular interface and shall take this value as an approximative measure of the density of defect states at Fe-ZnSe interfaces.

Finally, we state that an Fe induced band bending in the ZnSe layer does not exert a major influence on the conductivity. Because of the low defect concentration in ZnSe the bending would be of long range. However, the conductivity does not depend on the thickness of the ZnSe layer.

The coincidence of the transition temperatures of magnetic and transport measurements on Fe-ZnSe multilayers is obvious. Since the layers are produced the same way in both experiments it is conclusive that these transitions have the same origin. On one hand this transition makes the heat-induced antiferromagnetic coupling disappear, on the other hand it annihilates localized electron states at the interfaces. Therefore we conclude that interface defect states are responsible for the heat-induced exchange coupling.

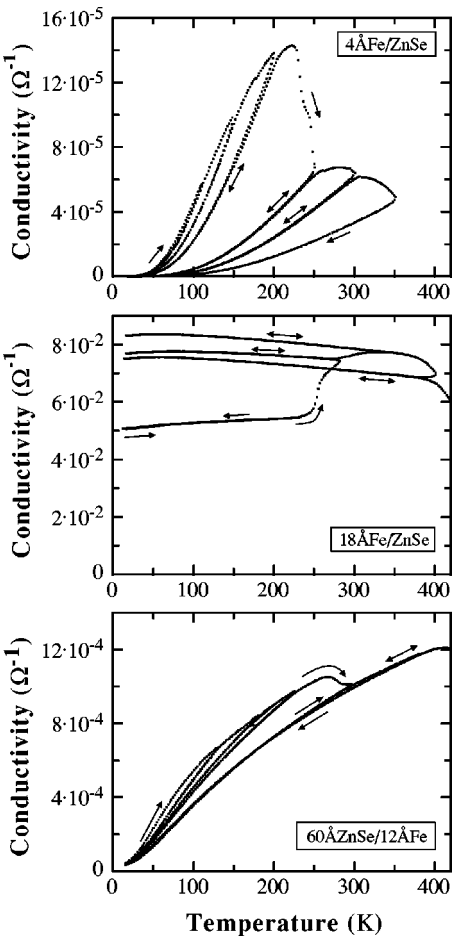

FIG. 8. Conductivity vs temperature measured along bilayers consisting of ZnSe and Fe evaporated at 30 K. The samples are stepwise annealed. Top panel: 4 Å Fe layer on 130 Å ZnSe; center panel: 18 Å Fe layer on 150 Å ZnSe; bottom panel: inverse bilayer, 60 Å ZnSe on 12 Å Fe layer. The course of the measurement is indicated by arrows.

While the existence, location, and density of the defect states could be identified, their relative position on the energy scale remains an open question. The present data do not include a contribution of free electron conduction, compare Eq. (5), which would determine E_C-E_S. Either this energy gap is too large or the parameter C is too small such as a contribution by free-electron conduction could be measured. Therefore alternative methods like photoemission should be applied.

Finally, the origin of the interface defect states remains a subject of speculations. We may state that rough interfaces lead to a higher stability of the defect states which is also evidenced by magnetic measurements.[24] Further, the replacement of Fe by Co does not alter the transition temperature. This indicates that the transition is governed by the structural stability of the ZnSe.

In order to stimulate the discussion we would like to suggest two possibilities which could stabilize defects at Fe-ZnSe interfaces:

• The metal-semiconductor interface may be strained which might lead to defects. The measured density $N(E_F)$

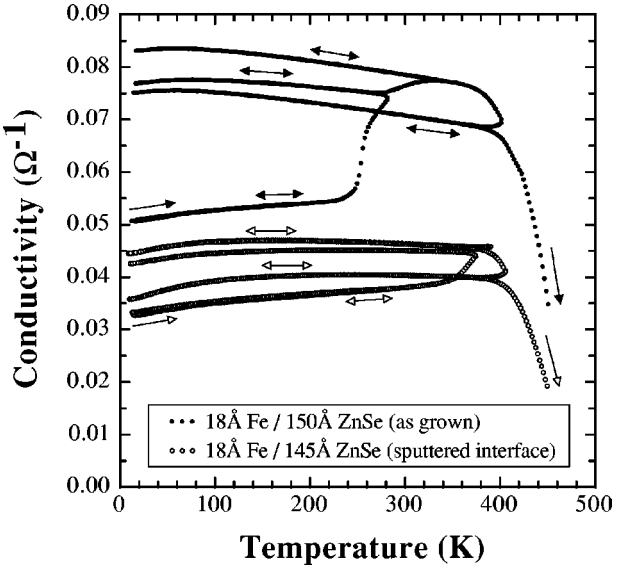

FIG. 9. Conductivity vs temperature measured along bilayers Fe/ZnSe with sputtered (empty dots) and as-grown (full dots) interfaces. All layers are evaporated at 30 K and stepwise annealed. The course of the measurement is indicated by arrows.

$\approx 1\times10^{13}$ eV^{-1} cm^{-2} and an assumed level width of $\Delta E_S \approx 0.1$ eV yields an estimate of the absolute density of defects of $N\approx10^{12}$ cm^{-2}. This means that there is a defect state every 100 Å. Strain takes several rows of atoms to be established and therefore this value supports the suggestion. Moreover, the annealing temperature can lead to small structural changes which in this case would be sufficient to annihilate the defects.

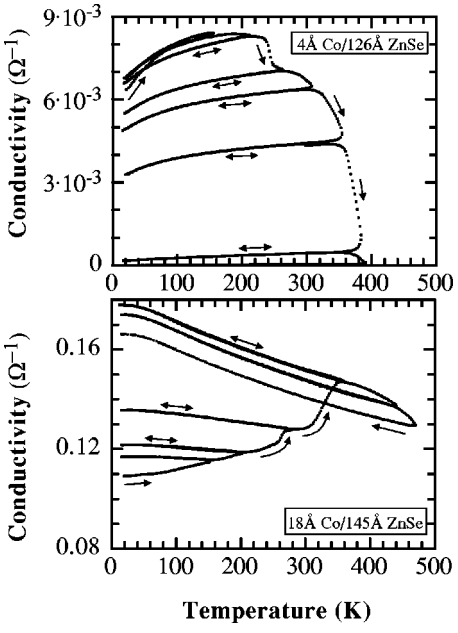

FIG. 10. Conductivity vs temperature measured along Co/ZnSe bilayers evaporated at 30 K. Top panel: 4 Å Co on ZnSe. Bottom panel: 18 Å Co on ZnSe. The samples are evaporated at 30 K and stepwise annealed. The course of the measurement is indicated by arrows.

• Fe impurities in ZnSe are known to be Fe^{3+} ions replacing Zn^{2+}.[25] This impurity obviously can bind an electron. However, the energy level of Fe donors in ZnSe is deep lying, about 1.7 eV below E_C,[26] which means that the extension of the donor orbital is small. This reduces the ability of long-range interaction which is necessary for the transmission of a magnetic exchange. If this donor is located close to an interface the nearby metal surface may influence the energy of the donor. One might think of a mirror charge established in the Fe layer which perturbs the donor and lifts its energy level. Co levels in ZnSe are even deeper lying ($E_C - E_S = 2.2$ eV),[27] which could be an explanation why in Co/ZnSe/Co trilayers heat-induced exchange has not been found.[28,29]

IV. MOLECULAR-ORBITAL MODEL

A. Requirements for the model

The knowledge of the importance of interface defect states for the occurrence of heat-induced effective exchange coupling gives us the inspiration to devise a corresponding model for the coupling. The concept of this model differs from any known description of magnetic coupling mechanisms in solid-state physics. However, the magnetic interaction of this model is analog to the spin interaction in chemical bindings. Therefore we call this concept ''molecular-orbital model.''

First of all, we briefly recall the requirements for a model of heat-induced exchange coupling. The model should lead to antiferromagnetic coupling across an amorphous, semiconducting spacer layer in the spacer-thickness range of about 20 Å. At the upper edge of this range the size of the interaction should decrease and finally disappear. At the lower edge the coupling should exhibit a ferromagnetic interaction. However, the occurrence of ferromagnetic coupling for very thin spacers is not decisive as in this thickness range other effects may be involved. Further, the temperature dependence of the coupling should result to be positive with a saturation behavior at temperatures around 100 K. It must be considered that the coupling does not depend on the semiconductor's energy gap, rather a dependence on the dielectric constant should appear.

Several earlier approaches have been made in order to model a coupling across semiconductors. So far, *k*-dependent tunneling,[30] direct tunneling,[31] resonant tunneling,[12] tunneling across defect states,[32] excitons in a direct band gap,[33] and quantum size effects in a double quantum well[34] have been studied. The coupling strength mediated by *k*-dependent or direct tunneling exponentially depends on the size of the semiconductors energy gap. As well, a mediation by excitons in a direct band gap depends on the size of the band gap. Therefore these models do not apply. Resonant tunneling, however, is able to describe an interaction with a positive temperature behavior, even a saturation behavior results. Still, it remains unclear how an antiferromagnetic interaction within an isolated range of spacer thickness shall be explained. Size effects in a double quantum well can reproduce the thickness dependence of the coupling. However, the temperature coefficient turns out to be negative, moreover, the assumptions of the model do not fully coincide with the ex-

TABLE I. $N(E_F)$ for various annealing temperatures T_i calculated from best fits of the data presented in Fig. 8. Calculated with Eq. (4) setting $\alpha^{-1}=10$ Å.

4 Å Fe/130 Å ZnSe	
T_i [K]	$N(E_F)$[eV^{-1} cm^{-2}]
90	3.3×10^{13}
150	3.5×10^{13}
200	3.6×10^{13}
250	2.5×10^{13}
300	2.5×10^{13}
18 Å Fe/150 Å ZnSe	
T_i [K]	$N(E_F)$[eV^{-1} cm^{-2}]
120	5.0×10^{14}
180	4.5×10^{14}
60 Å ZnSe/12 Å Fe	
T_i [K]	$N(E_F)$[eV^{-1} cm^{-2}]
130	2.4×10^{14}
180	2.4×10^{14}
230	2.3×10^{14}
300	2.1×10^{14}
380	2.1×10^{14}
450	2.0×10^{14}

perimental situation. Finally, the work on tunneling across defect states claims to explain antiferromagnetic coupling with a spacer thickness dependence in agreement with the experiment. However, the line of arguments is unclear and the report does not treat the temperature dependence of the coupling.

Shallow interface defect states which interfere across the spacer layer, on the other hand, do not depend on the size of the energy gap and therefore fulfill an important requirement so far. In the remainder of this section we sketch the concept of the molecular-orbital model, we present an approximate calculation, and we compare the calculated results with the experimental data.

B. Coupling mechanism

Let us consider an amorphous semiconductor layer of thickness d embedded between two ferromagnetic metal layers of thickness much larger than d. The semiconducting material is characterized by a dielectric constant ε and a reduced mass m^*. The defect states in the semiconductor bulk material are neglected at a first step. The ferromagnetic metal layers are characterized by a spin polarized free-electron gas and a chemical potential μ. At the interfaces localized electron states shall be present in the semiconducting material. We assume these electron states to be shallow donors and describe them as ground states of hydrogenlike impurities. These states shall have large extensions due to the screening of the central charge by the dielectricity of the semiconductor. The extensions of these $1s$-like electron states are so large that they may overlap across the spacer layer and in this way mediate the effective exchange coupling between the ferromagnets. The density of donor states at one interface N, however, shall be low enough so that the donors do not interact along the interfaces.

Metal-semiconductor junctions cause Schottky barriers related with depletion layers. The trilayer considered in this model is no exception, a possible charge transfer between the metal layers and the semiconductor gives rise to electrical dipoles across the interfaces. Since d is small the effect of these dipoles can be approximated by a shift in energy between the band structures of the metal layers and the semiconductor.

The coupling mechanism is illustrated by the energy schemes depicted in Fig. 11. Two configurations with the magnetizations aligned parallel (FM) and antiparallel (AFM) are distinguished. On the two energy scales on each picture the relevant electron states at the two interfaces of the sample are shown. The horizontal scale not only includes spatial position but also density of states. ''Up'' and ''down'' spin states are placed to the right- and to the left-hand side of each energy scale, respectively. The spin polarized d-bands represent the relevant electron states of the ferromagnetic layers. The $s^*_{\uparrow(\downarrow)}$ states represent the shallow donor states. Levels of overlapping donor states are drawn in between the energy scales. μ finally is the chemical potential of the system. The mechanism of the coupling involves two magnetic interactions, namely the coupling of the donor states to the nearby ferromagnets at the interface and the coupling among overlapping donor states across the semiconductor.

First, we consider the magnetic coupling of the donor states with the nearby ferromagnet at the corresponding interface. The donor orbitals overlap the ferromagnetic layer considerably and therefore we describe this coupling in mean-field approximation by a strong exchange field, the Weiss field $\mathbf{H_w}$. The magnetic energy of an electron with magnetic moment $\mathbf{m}$ in this field is given by $E_m=-\mathbf{m}\cdot\mathbf{H_w}$. In the ground state, $\mathbf{m}$ is parallel to the field. A magnetic moment standing antiparallel to $\mathbf{H_w}$ thus gains an energy of $2mH_w$ relative to the ground state. A Weiss field is approximately $H_w\sim10^7$ Oe which yields $2mH_w$ to be of the order of 1 eV. At ambient temperatures this energy is huge compared to kT. Consequently, in Fig. 11 the s^* states with antiparallel moment are drawn at a highly elevated energy. The magnetic moments of the donor states are therefore strongly coupled and aligned parallel to the magnetization of the nearby ferromagnet. This allows us, even at ambient temperatures, to consider the magnetic and the donor-spin configurations to be always the same.

The exchange interaction between overlapping donor states is much weaker and therefore it is the decisive one. Because of the low density of donor states at each interface, we only have to consider the interaction across the spacer, i.e., of one pair of donor states situated at the two interfaces at opposite positions, let us say at the ''right'' and at the ''left'' interface. The Pauli principle requires that the molecular-orbital wave function with parallel spins has a lower probability amplitude within the spacer layer than the

one with antiparallel spins. In Fig. 11 this consequence of quantum mechanics is symbolically represented with overlapping and separated circles for antiparallel and parallel spin configurations, respectively. This inequality causes an energy difference for interfering donors with different spin configurations which eventually drives the effective exchange coupling. In analogy with singlet and triplet states the level of antiparallel spin configuration is always lower than the one of parallel configuration. Therefore if all interfering donor states are occupied an antiferromagnetic coupling is preferred.

However, if all interfering donor states are empty no coupling results. The temperature dependence of the effective coupling strength J thus is a consequence of thermal repopulation of the donor states. In this thermodynamical picture the Fe layers are the particle reservoirs with chemical potential μ.

Let us roughly and qualitatively estimate the results of this model. In a range of spacer thickness where the donor states interfere an energy difference is caused and antiferromagnetic coupling prevails. At spacer thicknesses larger than the extension of the donor states there is no interference and therefore no coupling should be found. If μ is lower than the level of the donor states, as depicted in Fig. 11, there are no interfering donor states at 0 K and no coupling should result. With rising temperature these states get occupied by thermal excitation and the coupling strength increases. At some temperature, depending on the relative position of μ and the donor levels, a maximum share of donor states is occupied and the coupling strength saturates.

C. An approximate calculation

The mathematical description of the molecular-orbital model is developed in two steps. First, we calculate the relative energies of the electron states which are relevant for the coupling mechanism. We separately consider the two configurations with the magnetizations aligned parallel and antiparallel. Second, we calculate the occupation of these levels for the two configurations. Subtracting the resulting energies of the two configurations we eventually acquire an equation for the effective coupling strength J.

The relevant energies for the coupling are the donor levels and the chemical potential μ. The unperturbed donor levels E_S do not depend on the spin configuration while the levels of interfering donors $E_{\uparrow\downarrow}$ and $E_{\uparrow\uparrow}$ are determined by the configuration of their spins.

In order to calculate the energy levels of the shallow donors we neglect the Weiss fields and the nearby metallic surfaces and treat the donors as hydrogenlike atoms with two corrections, namely the screening factor ε and the reduced mass m^*. The standard Hamiltonian for shallow donors reads[35]

$$H_S=\frac{\hbar^2}{2m^*}\nabla^2-\frac{e^2}{\varepsilon r} \tag{6}$$

of which the ground state is a $1s$-like orbital,

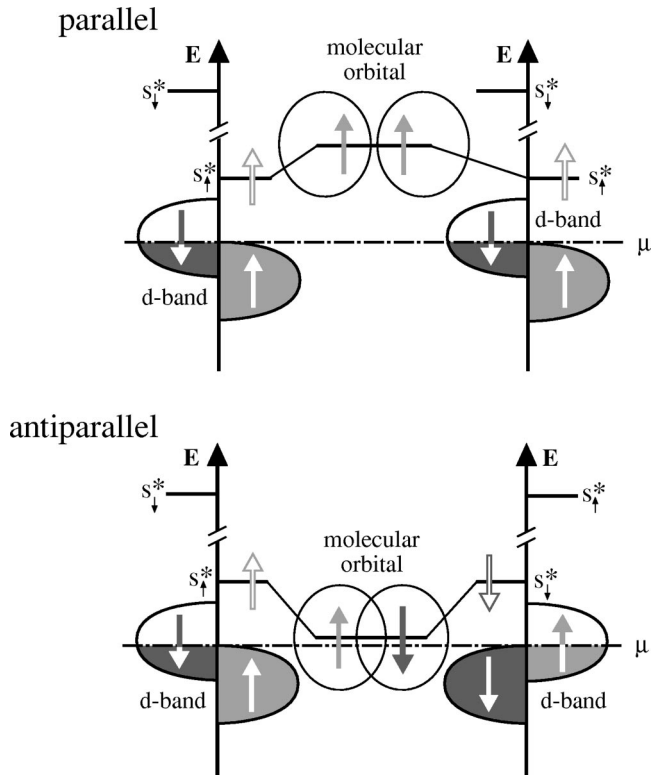

FIG. 11. The molecular-orbital model. On the energy scales the states at the ''left'' and ''right'' interfaces of two ferromagnetic layers separated by a semiconducting spacer layer are shown. Parallel and antiparallel alignments of the magnetizations are distinguished in the upper and lower parts, respectively. The horizontal axis shows spatial position and density of states. The spin-split d bands represent the ferromagnets, $s^*_{\uparrow(\downarrow)}$ are the donor states at the interfaces, and μ is the chemical potential. The levels between the energy scales are overlapping donor states forming molecular orbitals in the spacer. The energies of these molecular orbitals depend on the spin configuration which gives rise to the effective exchange coupling.

$$\phi(\varepsilon,m^*)\sim\left(\frac{m^*}{m\varepsilon a_0}\right)^{3/2}\cdot\exp\left\{-\frac{m^*r}{m\varepsilon a_0}\right\}, \tag{7}$$

where $a_0=0.52$ Å is the Bohr radius. The corresponding energy is

$$E_S=\frac{m^*}{m}\frac{1}{\varepsilon^2}E_0, \tag{8}$$

where $E_0=-13.6$ eV is the Rydberg energy.

A modified Bohr radius a_S may be defined as $a_S=a_0\cdot\varepsilon\cdot m/m^*$. The introduction of a screening factor $\varepsilon>1$ and a reduced mass $m^*<m$ obviously enlarges the spatial extension of the impurity states, as required. We note that the variation of both parameters qualitatively has the same effect. Therefore, for the sake of simplicity, we choose $m^*=m$ and only retain ε as a *free parameter*. Because of their large spatial extensions the donor orbitals from the ''left'' and the ''right'' interface, indeed, may overlap across the semiconductor to form giant molecular orbitals.

For the calculation of the interfering levels we consider a pair of shallow donors situated at opposite positions at the "left" (L) and the "right" (R) interface. In order to develop Hamiltonian and wave functions the ferromagnetic layers are neglected at a first step. This allows us to follow the *molecular-orbital method*.[36]

The Hamiltonian consists of Coulomb interactions only, i.e., of the single electron energies $H_{S,L}$ and $H_{S,R}$, where L and R denote "left" and "right," and of the Coulomb interactions across the spacer layer. The electrons are labeled 1 and 2, and $r_{j,i}$ stands for the distance $|\mathbf{r_j}-\mathbf{r_i}|$ with $j=R$, L, and $i=1,2$.

$$H=H_{S,L}+H_{S,R}+\frac{e^2}{\varepsilon}\left(-\frac{1}{r_{L,2}}-\frac{1}{r_{R,1}}+\frac{1}{r_{1,2}}+\frac{1}{d}\right). \tag{9}$$

For the wave functions the orbitals $\phi_L(r)$ and $\phi_R(r)$ are combined to *bonding* and *antibonding* molecular orbitals, respectively:

$$\psi_{+,\sigma}(r,s)\sim[\phi_L+\phi_R](r)\chi_\sigma(s), \tag{10}$$

$$\psi_{-,\sigma}(r,s)\sim[\phi_L-\phi_R](r)\chi_\sigma(s). \tag{11}$$

$\chi_\sigma(s)$ denotes the spin-wave function with $\sigma=\uparrow,\downarrow$ and s is the z component of the spin with the values $\uparrow,\downarrow$. The value of the spin-wave functions is $\chi_\uparrow(\uparrow)=1$, $\chi_\downarrow(\downarrow)=1$, and zero otherwise. A Slater determinant combining two bonding orbitals leads to the well-known singlet state. On the other hand, a combination of a bonding and an antibonding orbital yields the triplet state.[37]

These wave functions are heavily perturbed if each of the donors interacts with the magnetization of a nearby ferromagnet. Close to the interfaces the electrons experience the Weiss fields. Their energy is lowered by the magnetic energy $E_m=\mathbf{mH_w}$ if their magnetic moment $\mathbf{m}$ is aligned parallel to the respective Weiss field. Outside the ferromagnetic layer $\mathbf{H_w}$ decreases rapidly such that the electrons have an elevated amplitude towards the respective interface. Particularly in the case of antiparallel alignment of the magnetizations, the symmetry of the molecular orbitals is broken.

In order to take this perturbation into account we introduce two parameters α and β into the molecular orbitals. Because of the broken symmetry we have to consider two linear combinations of the bonding and antibonding orbitals, Eqs. (10) and (11), respectively:

$$\psi_{L,\sigma}(r,s)=[\alpha\phi_L+\beta\phi_R](r)\chi_\sigma(s), \tag{12}$$

$$\psi_{R,\sigma}(r,s)=[\beta\phi_L+\alpha\phi_R](r)\chi_\sigma(s). \tag{13}$$

The parameters α and β would have to be optimized now. For the sake of simplicity and for a very first approximation we set $\alpha=1$ and $\beta=0$. $\psi_{L,\sigma}(r,s)$ and $\psi_{R,\sigma}(r,s)$ combined in a Slater determinant lead to the wave functions for antiparallel and parallel alignment, $\Psi_{\uparrow\downarrow}$ and $\Psi_{\uparrow\uparrow}$, respectively. Note that these wave functions are completely different from the well-known singlet and triplet states and that there exists only one wave function for each magnetic alignment,

$$\Psi_{\uparrow\downarrow}(1,2)=\frac{1}{\sqrt{2}}[\phi_L(1)\chi_\uparrow(1)\phi_R(2)\chi_\downarrow(2)-\phi_L(2)\chi_\uparrow(2)\phi_R(1)\chi_\downarrow(1)], \tag{14}$$

$$\Psi_{\uparrow\uparrow}(1,2)=\frac{1}{\sqrt{2(1-S^2)}}\chi_\uparrow(1)\chi_\uparrow(2)[\phi_L(1)\phi_R(2)-\phi_L(2)\phi_R(1)], \tag{15}$$

where S is the overlap integral $\int\phi_L(r)\phi_R(r)d^3r$. The derived wave functions [Eqs. (14) and (15)] and the Hamiltonian [Eq. (9)] allow to calculate the energies for antiparallel and parallel alignment $E_{\uparrow\downarrow}$ and $E_{\uparrow\uparrow}$,

$$E_{\uparrow\downarrow}=E_S(\varepsilon)+\frac{1}{2}\left[\frac{e^2}{\varepsilon d}+V_c(d,\varepsilon)\right], \tag{16}$$

$$E_{\uparrow\uparrow}=E_S(\varepsilon)+\frac{1}{2}\left[\frac{e^2}{\varepsilon d}+\frac{V_c(d,\varepsilon)-V_{ex}(d,\varepsilon)}{1-S^2(d,\varepsilon)}\right]. \tag{17}$$

V_c and V_{ex} are the Coulomb and exchange energies, respectively,

$$V_c=\int\int\phi_L^2(r_1)\phi_R^2(r_2)\frac{e^2}{\varepsilon}\left(-\frac{1}{r_{L,2}}-\frac{1}{r_{R,1}}+\frac{1}{r_{1,2}}\right)d^3r_1d^3r_2, \tag{18}$$

$$V_{ex}=\int\int\phi_L(r_1)\phi_R(r_2)\frac{e^2}{\varepsilon}\left(-\frac{1}{r_{L,2}}-\frac{1}{r_{R,1}}+\frac{1}{r_{1,2}}\right)\times\phi_L(r_2)\phi_R(r_1)d^3r_1d^3r_2. \tag{19}$$

The orbitals $\phi_{L(R)}$ are inserted from Eq. (7). We resolve V_c and V_{ex} using the integrals by Sugiura[38] and then numerically evaluate $E_{\uparrow\downarrow}$ and $E_{\uparrow\uparrow}$ with the free parameter $\varepsilon=10$, which roughly corresponds to the value of ZnSe. The results are compiled in Fig. 12.

The relative position of the chemical potential μ is not easy to determine. As mentioned, a charge transfer at the metal-semiconductor junction may result in a shift of the respective energy structures. The dependence of this shift on the electronic structures of the materials, additional influences of metal-induced gap states, interface, and bulk defect states are still a subject of discussion.[39] Therefore we use $E_S-\mu$ as the *second free parameter* of the model, represented in Fig. 12 as a broken line at a physically meaningful position.

The compiled energies in Fig. 12 already indicate the behavior of J. As $E_{\uparrow\downarrow}$ is always lower than $E_{\uparrow\uparrow}$ antiferromagnetic coupling is expected to predominate. $E_{\uparrow\downarrow}$ has a characteristic minimum which for $\varepsilon=10$ occurs at about 10 Å. In this range the donors are most likely occupied and if the minimum is lower than μ, as suggested in Fig. 12, antiferromagnetic coupling occurs already at 0 K. A variation of ε to smaller and larger values shifts the energy minimum to shorter and longer distances, respectively. The value of the energy minimum relative to E_S is not accurate as the levels of interfering donors are calculated in rough approximation.

For the Slater determinant, we use orbitals ϕ of which the amplitude is centered only at the position of one donor; i.e., we set the parameters $\alpha=1$ and $\beta=0$. However, if we apply valence-bond theory, which combines orbitals with finite amplitude at both donor positions ($\alpha=\beta$), the contribution of the exchange energy is larger and the energy minimum for $E_{\uparrow\downarrow}$ results to be much deeper. The singlet and triplet wave functions and the wave functions derived in this paper [Eqs. (14) and (15)], respectively, are expected to approximate the precise molecular-orbital wave function from two extremal points. Therefore we expect the energy minimum of an improved approximation with optimized parameters α and β to be lower than the one in the present case.

The coupling strength J depends on the population of the energy levels. In order to maintain overall charge neutrality we must allow for transfer of electrons from or to the metal layers, which serve as particle reservoirs. We therefore have to consider the thermodynamic potential $\Omega=\Sigma_i n_i E_i - \mu\Sigma_i n_i$, where E_i are the one particle energies E_S, $E_{\uparrow\downarrow}$, and $E_{\uparrow\uparrow}$ and n_i their respective occupations. The effective coupling strength J, which phenomenologically is defined in Eq. (1), is identified with the difference of the thermodynamic potentials per unit area A.[5]

$$J=\frac{1}{A}(\Omega_{\uparrow\downarrow}-\Omega_{\uparrow\uparrow}), \tag{20}$$

$\Omega_{\uparrow\downarrow}$ and $\Omega_{\uparrow\uparrow}$ are the thermodynamic potentials for the respective spin configurations.

The occupations n_i, on one hand, are governed by the Fermi distribution $f(E_i)=[1+\exp\{(E_i-\mu)/kT\}]^{-1}$ since the interfering electrons still are fermions. On the other hand, n_i strongly depend on the density of donor states at one interface N. Basically, the occupation may be considered as the available states of a specific energy level $N^*(E_i)$ weighted by the Fermi distribution, $n_i=N^*(E_i)f(E_i)$. However, $N^*(E_i)$ cannot simply be identified with $2N$, the density of donor states at the two interfaces. The reason is that electrons may have different energies on the very same donor state. On one hand, the electron energy in a pair of potentially interfering donor states amounts to E_S for single occupation. On the other hand it equals $E_{\uparrow\downarrow}$ or $E_{\uparrow\uparrow}$ for double occupation, depending on the spin configuration. In order to properly account for this we first make all donor states at both interfaces available and calculate the share of doubly occupied donor pairs,

$$n_{\uparrow\downarrow(\uparrow\uparrow)}=2Nf(E_{\uparrow\downarrow,(\uparrow\uparrow)}). \tag{21}$$

In a second step the remaining empty donor states are made available for single occupation. As single occupation means that only one state of a pair is populated, hence N^* contains N once and further a prefactor which withdraws the states which have been doubly occupied,

$$n_S=[1-f(E_{\uparrow\downarrow(\uparrow\uparrow)})]Nf(E_S). \tag{22}$$

N is treated as the *third free parameter* of the model.

With the knowledge of the occupations we may write the thermodynamical potentials $\Omega_{\uparrow\downarrow}$ and $\Omega_{\uparrow\uparrow}$,

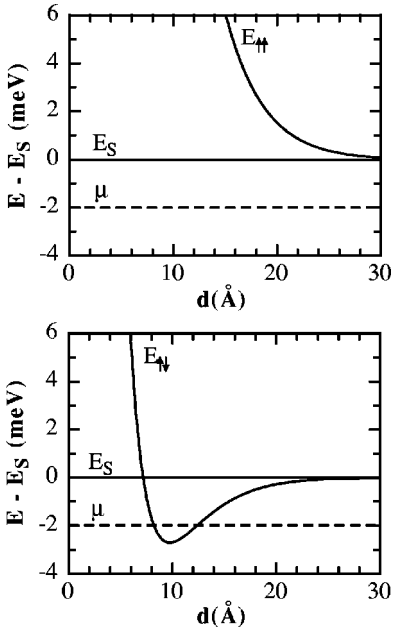

FIG. 12. Calculated energy levels versus distance between the interfering donors for parallel (top panel) and antiparallel (bottom panel) spin configurations, respectively. The free parameter ε is chosen to be 10, which roughly corresponds the dielectric constant of ZnSe ($\varepsilon_{ZnSe}=9.2$). $E_{\uparrow\downarrow(\uparrow\uparrow)}$ are the energies of interfering electrons, E_S is the energy of a noninteracting donor state, set to zero, and μ is the chemical potential. $E_S-\mu$ is treated as a free parameter.

$$\Omega_{\uparrow\downarrow(\uparrow\uparrow)}=AN\{2f(E_{\uparrow\downarrow(\uparrow\uparrow)})[E_{\uparrow\downarrow(\uparrow\uparrow)}-\mu] + [1-f(E_{\uparrow\downarrow(\uparrow\uparrow)})]f(E_S)[E_S-\mu]\}. \tag{23}$$

Introducing $\Omega_{\uparrow\downarrow}$ and $\Omega_{\uparrow\uparrow}$ into Eq. (20) we finally get an equation for the coupling strength J.

$$J=N\{2f(E_{\uparrow\downarrow})[E_{\uparrow\downarrow}-\mu]-2f(E_{\uparrow\uparrow})[E_{\uparrow\uparrow}-\mu] + [f(E_{\uparrow\uparrow})-f(E_{\uparrow\downarrow})]f(E_S)[E_S-\mu]\}. \tag{24}$$

We present numerical results of J in Fig. 13 for one appropriate choice of the free parameters. The screening factor $\varepsilon=10$ lies in the range of the dielectric constant of ZnSe ($\varepsilon_{ZnSe}=9.2$). The density of defect states $N=1\times10^{12}$ cm^{-2} is realistic for this type of interfaces and it is supported by the transport measurements on Fe/ZnSe heterostructures (see Sec. III). The relative position of μ is freely chosen to be $E_S-\mu=2$ meV such that it corresponds to a characteristic temperature in the range of about 50 K. In Fig. 13 the dependences on the spacer thickness (top panel) as well as the temperature behaviors (bottom panel) are compiled.

D. Discussion

The numerical results presented in Fig. 13 agree amazingly well with the experimental data shown in Figs. 2 and 3. With a physically meaningful choice of the three free parameters, even in a roughly approximated calculation, we find the requirements for the model perfectly fulfilled. First of all,

the antiferromagnetic coupling occurs in a spacer-thickness range of about 10 Å which well corresponds to the experimental observations. At low temperatures this range is quite narrow and it broadens towards larger spacer thicknesses with rising temperature. For thick spacers we find weak or no coupling. At the lower edge of the antiferromagnetic thickness range ferromagnetic coupling is found. It does not completely predominate, at variance with the experimental observations. However, very thin spacers cannot be expected to perfectly separate the ferromagnetic layers. Therefore pinholes may occur and align the magnetizations parallel to each other. Eventually, it is hard to resist emphasizing the detail that even the heat-induced sign change, measured at the thicker edge of the antiferromagnetic range, is reproduced by the model for $d \approx 16$ Å. The calculated temperature dependences exhibit a positive temperature coefficient, which is the key feature of exchange coupling across amorphous semiconductors. In particular, one finds good agreement to the experimental data for larger spacer thicknesses; the coupling strength saturates above 100 K. Finally, the magnitude of the coupling strength is well reproduced, the calculated and experimental results turn out to be within the same order of magnitude: J amounts to 10^{-6} J m^{-2} at thermal saturation.

The quality of a model is indicated by the agreement of its results with the experimental data. However, the quality augments considerably if, upon a variation of the free parameters, the results behave in a physically meaningful way. In the present case, the easiest parameter to understand is the number of donors per interface area N. The coupling strength J is proportional to N, and thus a variation of N does not result in a qualitative change of J. As the chosen value of N is based on transport measurements, the reliability of the calculated magnitude of J is supported. The screening factor ε and the position of the chemical potential μ, in contrast, influence the thickness and temperature dependences of J. However, we wish to emphasize that the gross features of J persist upon a considerable variation of the free parameters, as is shown in Fig. 14. On one hand an increasing ε shifts the thickness range where the coupling occurs to larger spacer thicknesses and it reduces the coupling strength slightly, compare Fig. 14, panels (a) and (b). On the other hand the position of μ mainly influences the temperature dependence of J. The larger the energy gap $E_S - \mu$ the higher the temperature where J saturates; compare Fig. 14, panels (c) and (d).

In conclusion, we propose a molecular-orbital model of heat-induced exchange coupling between ferromagnetic layers separated by an amorphous-semiconductor spacer layer. The mechanism is based on the assumption of localized, weakly bound electron states to exist at the semiconductor-metal interfaces. They are described as ground states of hydrogenlike donors which are screened by the dielectricity of the semiconductor. They can form molecular orbitals across the spacer layer and thus mediate an exchange interaction. The present calculation, even with rough approximations, yields good agreement with the experimental data. Moreover, the calculated results behave quite stable upon variation of the free parameters. Hence we are confident that the molecular-orbital model will persuade as a valuable description of heat-induced effective exchange coupling.

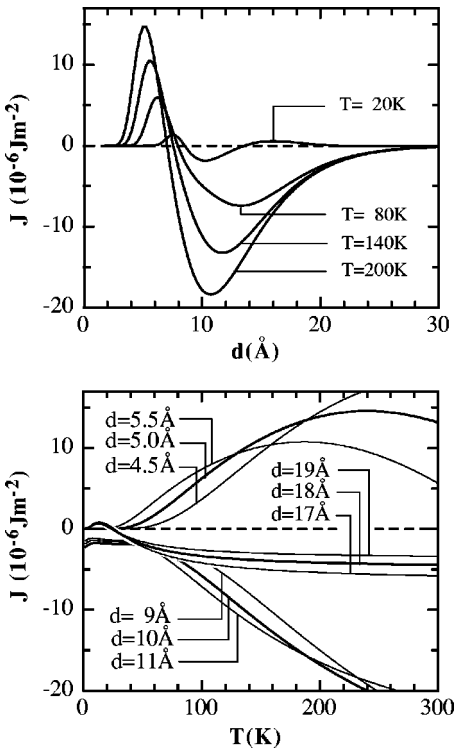

FIG. 13. Top panel: Calculated effective coupling strength J vs spacer thickness d for various temperatures. Bottom panel: Calculated effective coupling strength J vs temperature T for various spacer thicknesses. For all calculations the free parameters are set $N = 1 \times 10^{12}$ cm^{-2}, $\varepsilon = 10$, and $E_S - \mu = 2$ meV.

V. SUMMARY AND OUTLOOK

The molecular-orbital model presents a different concept of a magnetic coupling. However, it is calculated in the roughest approximation. Therefore it is expected to stimulate further theoretical activity.

The most interesting task is the precise description of the interfering donor wave functions, the molecular orbitals. As stated in Sec. IV C we work in a very first approximation. An optimization of the parameters α and β or even a new description would lead to a better calculation of the exchange energies. On the same footing the description of the single donor states should be improved. The influence of the nearby metal layer has to be considered which will perturb the geometry and the energy of the donor states. It is to be expected that the donor levels do not form singular distributions. A finite width of the energy distribution will mainly correct the coupling behavior at low temperatures.

The theoretical work needs to be supported by experimental evidence of the origin of the donor states. For example, this origin could be unveiled by an artificial implantation of impurities which are expected to form shallow donors. In order to get these impurities close to the interfaces, as requested by the model, one would have to evaporate the multilayer like a good Italian lasagne. A submonolayer of the

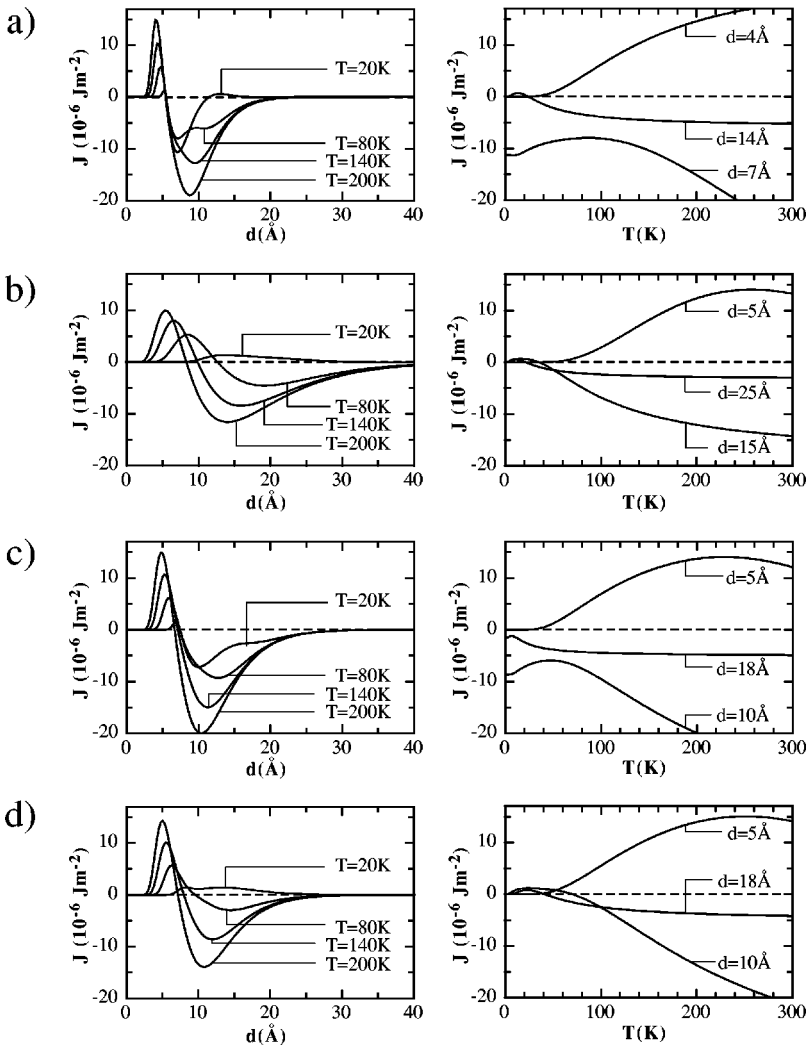

FIG. 14. Calculated effective coupling strength J vs spacer thickness d (left panels), and vs temperature T (right panels) under variation of the free parameters ε and $E_S-\mu$. (a) $\varepsilon=7$, $E_S-\mu=2$ meV. (b) $\varepsilon=15$, $E_S-\mu=2$ meV. (c) $\varepsilon=10$, $E_S-\mu=0$ meV. (d) $\varepsilon=10$, $E_S-\mu=4$ meV. The density of defect states $N=1\times10^{12}$ cm^{-2} is held constant for all calculations.

impurities has to be evaporated between the ferromagnetic and the semiconductor layer like cheese crumbs sprinkled between the pasta sheets and the tomato sauce. This sample may be expected to be stable at room temperature and it could be examined by photoemission, for example. The experiment is also of technical interest because the stability at room temperature is a necessity for an application of heat-induced exchange coupling in technical devices.

The insight that the population of interface donor states, which in the present case is governed by thermal excitation, causes magnetic coupling leads to the question of whether this population and hence the coupling also could be influenced by an applied voltage. A *voltage-controlled exchange coupling*, eventually, would definitely have great potential for powerful technical applications.

ACKNOWLEDGMENTS

We would like to thank H. C. Siegmann for continuous support and stimulating conversations, and K. Brunner for expert technical assistance. With great pleasure we acknowledge many helpful comments by W. Baltensperger and J. W. Blatter. Financial support by the Schweizerischer Nationalfonds is gratefully acknowledged.

[1] Known as the RKKY interaction, M. A. Ruderman and C. Kittel, Phys. Rev. **96**, 99 (1954); T. Kasuya, Prog. Theor. Phys. **16**, 45 (1956); K. Yoshida, Phys. Rev. **106**, 893 (1957).

[2] P. Grünberg, R. Schreiber, Y. Pang, M. B. Brodsky, and H. Sowers, Phys. Rev. Lett. **57**, 2442 (1986).

[3] S. S. P. Parkin, N. More, and K. P. Roche, Phys. Rev. Lett. **64**, 2304 (1990).

[4] J. Unguris, R. J. Celotta, and D. T. Pierce, Phys. Rev. Lett. **67**, 140 (1991).

[5] D. M. Edwards, J. Mathon, R. B. Muniz, and M. S. Phan, Phys. Rev. Lett. **67**, 493 (1991).

[6] W. Baltensperger and J. S. Helman, Appl. Phys. Lett. **57**, 2954 (1990).

[7] P. Bruno and C. Chappert, Phys. Rev. Lett. **67**, 1602 (1991).

[8] S. Toscano, B. Briner, H. Hopster, and M. Landolt, J. Magn. Magn. Mater. **114**, L6 (1992).
[9] B. Briner and M. Landolt, Phys. Rev. Lett. **73**, 340 (1994).
[10] P. Walser, M. Schleberger, P. Fuchs, and M. Landolt, Phys. Rev. Lett. **80**, 2217 (1998).
[11] P. Walser, M. Hunziker, T. Speck, and M. Landolt, Phys. Rev. B **60**, 4082 (1999).
[12] Beat Briner, Ph.D. thesis, ETH Zürich, 1994.
[13] Peter Walser, Ph.D. thesis, ETH Zürich, 1998.
[14] M. Hunziker and M. Landolt, Surf. Sci. **468**, 187 (2000).
[15] M. Hunziker and M. Landolt, Phys. Rev. Lett. **84**, 4713 (2000).
[16] B. T. Jonker and G. A. Prinz, J. Appl. Phys. **69**, 2938 (1991).
[17] P. K. Lim and D. E. Brodie, Can. J. Phys. **55**, 1641 (1977).
[18] M. Landolt, Appl. Phys. A: Solids Surf. **A41**, 83 (1986).
[19] H. C. Siegmann, J. Phys.: Condens. Matter **4**, 8395 (1992).
[20] Cf. *CRC Handbook of Chemistry and Physics*, 69th ed. (CRC Press, Boca Raton, 1989).
[21] M. Schleberger, P. Walser, M. Hunziker, and M. Landolt, Phys. Rev. B **60**, 14 360 (1999).
[22] N. F. Mott and E. A. Davis, *Electronic Processes in Noncrystalline Materials* (Clarendon Press, Oxford, 1979).
[23] B. T. Jonker, G. A. Prinz, and Y. U. Idzerda, J. Vac. Sci. Technol. B **9**, 2437 (1991).
[24] Simon Haas (unpublished).
[25] J. Dieleman, Philips Res. Rep. **20**, 206 (1965).
[26] J. Dieleman, J. W. de Jong, and T. Meijer, J. Chem. Phys. **45**, 3178 (1966).
[27] J. M. Noras, H. R. Szawelska, and J. W. Allen, J. Phys. C **14**, 3255 (1981).
[28] Thomas Speck (unpublished).
[29] Susanne Rechsteiner (unpublished).
[30] J. C. Slonczewski, Phys. Rev. B **39**, 6995 (1989).
[31] P. Bruno, Phys. Rev. B **49**, 13 231 (1994).
[32] M.-W. Xiao and Z.-Z. Li, Phys. Rev. B **54**, 3322 (1996).
[33] C. A. R. Sá de Melo, Phys. Rev. B **51**, 8922 (1995).
[34] J.-Z. Wang and B.-Z. Li, Phys. Rev. B **59**, 6383 (1999).
[35] For example, see N. W. Ashcroft and N. D. Mermin, *Solid State Physics* (Saunders College Publishing, Orlando, 1976).
[36] Compare any textbook, i.e., G. Baym, *Lectures on Quantum Mechanics* (Addison-Wesley Publishing, Redwood City, 1969).
[37] W. Heitler and F. London, Z. Phys. **44**, 455 (1927).
[38] Y. Sugiura, Z. Phys. **45**, 484 (1927).
[39] For example, see W. Mönch, *Electronic Structure of Metal-Semiconductor Contacts* (Kluwer Academic Publishers, Dorderecht, 1990).